Electroosmotic Flows in Channel with Two Symmetric Periodic Arrays of Square-Sectioned Ribs

Sangmo Kang*, Yong Kweon Suh
Department of Mechanical Engineering, Dong-A University, Busan 604-714, Korea

The present study has numerically investigated two-dimensional electroosmotic flows in channel equipped with two symmetric periodic arrays of square-sectioned ribs with one-fifth of the channel half-width in size. For the simulation, the ionic-species and electric-potential equations as well as the continuity and momentum ones are solved using the finite volume method. Instead of assuming the Boltzmann distribution, the Nernst-Plank equation is applied for the ionic species. Results show that the steady electroosmotic flow and ionic distributions depend strongly on the EDL length and streamwise periodic length. For a sufficiently large periodic length, the fluid flows along the wall as in the inviscid flow at a small EDL length compared with the rib size, whereas it flows with involving two recirculation bubbles around the rib as in the pressure-driven flow at a large EDL length. At an intermediate EDL length comparable to the rib size, a very intricate flow pattern is observed around the rib. With decreasing periodic length, on the other hand, the interaction between two adjacent ribs gets stronger and thus the flow pattern significantly changes. This study would contribute to further understanding electroosmotic flows in micro- and nanofluidic devices of complicated geometries.

Key Words: Electric Double Layer (EDL), Electroosmotic Flows, Square-Sectioned Ribs, Overlapped EDL

Nomenclature

C_s, C_0 : Molar ionic concentrations
D_s, D : Ionic diffusion coefficients
E_0 : Mean external electric field
H : Channel half-width
h : Rib size
L_p : Streamwise periodic length
Pe : Peclet number
P, p : Pressures
Sc : Schmidt number
t : Time
U_{eo} : Electroosmotic velocity
u_i : Velocity components
x_i : Cartesian coordinates
z_s, z : Ionic valences
Δ : Increment
ε : Fluid permittivity
ζ_0 : Zeta potential
ζ_0^* : Nondimensional zeta potential
κ : Nondimensional EDL length
λ : EDL length
ρ_e : Volumetric electric-charge density
σ_0 : Surface electric-charge density
Φ : Total electric potential
ϕ, ϕ' : External electric potentials
ψ, ψ_w : Electric potentials due to the EDL
Ω : Parameter $[=(-\zeta_0)/(-E_0H)]$

Subscripts

i : Indices (1,2)

* Corresponding Author,
E-mail : kangsm@dau.ac.kr
TEL : +82-51-200-7636; **FAX** : +82-51-200-7656
Department of Mechanical Engineering, Dong-A University, Busan 604-714, Korea. (Manuscript **Received** November 20, 2006; **Revised** December 5, 2006)

m : Anions
p : Cations
s : Indices (p, m)

1. Introduction

With the advent of micro- and nanofluidic devices, the electrokinetics has drawn increasingly more attention because of its feasibility and efficiency for controlling microflows in a variety of applications: for example, lab-on-a-chip, sensors and actuators, and analytical chemistry. A solid surface in contact with an infinitely large extent of electrolyte solution inherits a certain amount of charges on the surface, either by ionization of a surface group or by ion adsorption, while the counterions are released into the solution. It leads to formation of the electric double layer (EDL) immediately next to the surface, with a net amount of excess-counterion charges that electrically counterbalance the surface charges. The excess counterions in the EDL move by an externally applied electric field and then drive the surrounding fluid in the EDL to move with them. Subsequently, the fluid motion in the EDL drags the fluid outside of the EDL to also move due to the fluid viscosity, finally resulting in a bulk fluid motion. Such an electrokinetic phenomenon is called the electroosmosis. Here, the characteristic thickness of the EDL, λ, often called the Debye shielding distance or EDL length, depends on the ionic concentration in the bulk of the fluid and is typically at nano scales [see Li (2004) for more details]. Recently, the electroosmosis has been investigated by many researchers as a promising tool in micro- and nanofluidic devices not only for delivering bulk of the fluid, but also for enhancing its mixing efficiency.

Mixing of fluids is an important process in designing micro- or nanofluidic devices in the field of, particularly, biotechnology such as μ-TAS (micro total analysis systems) or lab-on-a-chip. However, feasible and efficient mixing cannot be achieved easily because flows in these devices are unavoidably laminar due to low Reynolds numbers and thus mixing depends solely on the molecular diffusion (Stroock et al., 2002). To enhance the mixing efficiency, therefore, there must be transverse components of flow that can stretch and fold bulk of the fluid over the cross section of the device. There are two general strategies for generating such transverse flows: passive methods in which transverse flows result from the interaction of the externally driven flow with the fixed channel geometry, and active methods in which transverse flows are generated by oscillatory forcing within the channel (Stone et al., 2004). The passive mixing utilizes no energy input except the mechanism used to drive the fluid flow, whereas the active mixing exerts some form of active control over the flow field through such means as moving parts or varying electric fields (Liu et al., 2000). While the active mixers can produce excellent mixing, they are often difficult to fabricate, operate, clean, and integrate into microfluidic systems. Thus, in many cases, passive mixers have been more interesting because they are relatively simple to implement. The present study is mainly concerned with one of the issues that are closely related to the passive mixing: electroosmotic flows in channel equipped with two symmetric periodic arrays of square-sectioned ribs.

Quite a few numerical studies have been performed on the electroosmotic flow, but mainly in relatively simple geometries (Patankar and Hu, 1998; Qu and Li, 2000; Lin et al., 2002; Li, 2004; Kwak and Hasselbrink, 2005). In addition, most of them investigated electroosmotic flows for the very small EDL length in comparison with the channel half-width, assuming that the Boltzmann distribution was already established for the ionic species. Therefore, they had to confine themselves to the nonoverlapped EDL case. By contrast, exceptions can be found in Lin et al. (2002) and Kwak and Hasselbrink (2005). They adopted the Nernst-Plank equation and the full Navier-Stokes equation without any assumption of the Boltzmann distribution in the modelling of electroosmotic flow in micro- or nanofluidic devices. Despite their excellent achievements, their flow geometries were relatively simple, for example crossed plane channels for Lin et al. (2002) and a plane channel for Kwak and Hasselbrink (2005). Note that the flow geometry is seldom so simple

in real applications. Therefore, numerical approaches without any Boltzmann-distribution assumption have to be extended to the electroosmotic flow of more complicated geometry. It is a main motivation of the present study.

The objectives of the present study are to numerically investigate two-dimensional electroosmotic flows in channel equipped with two symmetric periodic arrays of square-sectioned ribs. Such a flow geometry is chosen because transverse flows can be generated due to the interaction between the electrically driven flow (electroosmotic flow) and the arrays of square-sectioned ribs, which may finally enhance the mixing efficiency. For the numerical study, the ionic-species and electric-field equations as well as the continuity and momentum ones are solved using the finite volume method. Note that, instead of assuming the Boltzmann distribution, the Nernst-Plank equation is applied for the ionic species. This study would contribute to further understanding electroosmotic flows and developing more feasible passive mixers in micro- and nanofluidic devices.

2. Numerical Method

Numerical simulations are performed on two-dimensional incompressible electroosmotic flows of a dilute two-species electrolyte in channel which is equipped with two symmetric periodic arrays of square-sectioned ribs and whose wall is made of dielectric materials. For the simulations, it is assumed that the electrolyte solution is symmetric, that is the cations and anions have the same physical and chemical properties. The schematic diagram of the flow geometry and computational domain is shown in Fig. 1. Here, h and L_p denote the rib size and streamwise periodic length, respectively, and they are nondimensionalized by the channel half-width, H. For the computational convenience, the Cartesian coordinate system, (x_1, x_2), is adopted with an original point at the front bottom corner of a rib.

The appropriate governing equations for the flow field and ionic distributions are written (Patankar and Hu, 1998 ; Hu et al., 1999 ; Lin et al., 2004 ; Kwak and Hasselbrink, 2005 ; Qian and Bau, 2005), in a nondimensional form, as

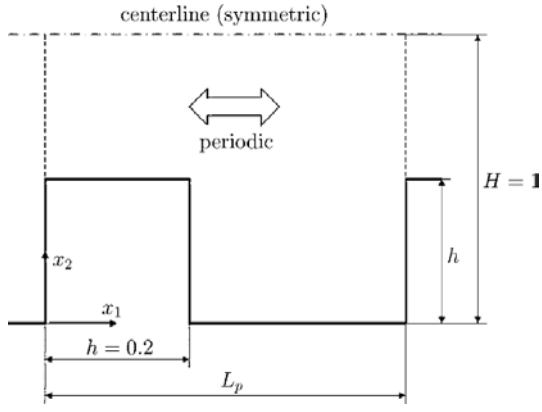

Fig. 1 Schematic diagram of the flow geometry and computational domain. Note that all the lengths are nondimensionalized by the channel half-width

$$\frac{\partial u_j}{\partial x_j}=0 \tag{1}$$

$$\frac{\partial u_i}{\partial t}+\mathrm{Pe}\frac{\partial u_i u_j}{\partial x_j} =-\mathrm{Sc}\frac{\partial p}{\partial x_i}+\mathrm{Sc}\frac{\partial^2 u_i}{\partial x_j \partial x_j}-\frac{\mathrm{Sc}}{2\kappa^2\zeta_0^*}\rho_e\frac{\partial \Phi}{\partial x_i} \tag{2}$$

$$\frac{\partial C_p}{\partial t}+\mathrm{Pe}\frac{\partial (C_p u_j)}{\partial x_j}=\frac{\partial^2 C_p}{\partial x_j \partial x_j}+\frac{\zeta_0^*}{\Omega}\frac{\partial}{\partial x_j}\left[C_p\frac{\partial \Phi}{\partial x_j}\right] \tag{3}$$

$$\frac{\partial C_m}{\partial t}+\mathrm{Pe}\frac{\partial (C_m u_j)}{\partial x_j}=\frac{\partial^2 C_m}{\partial x_j \partial x_j}-\frac{\zeta_0^*}{\Omega}\frac{\partial}{\partial x_j}\left[C_m\frac{\partial \Phi}{\partial x_j}\right] \tag{4}$$

$$\Phi=\phi+\frac{\Omega}{\zeta_0^*}\psi=[\phi'-x_1]+\frac{\Omega}{\zeta_0^*}\psi \tag{5}$$

$$\frac{\partial^2 \phi'}{\partial x_j \partial x_j}=0 \tag{6}$$

$$\frac{\partial^2 \psi}{\partial x_j \partial x_j}=-\frac{1}{2\kappa^2}\rho_e \tag{7}$$

$$\rho_e=C_p-C_m \tag{8}$$

where x_i's are the Cartesian coordinates and t the time. Here, u_i's are the velocity components, p the pressure, C_p and C_m the concentrations of the cations and anions, respectively, and ρ_e the volumetric electric-charge density. Note that the total electric potential, Φ, is decomposed into an electric potential due to the external electric field, $\phi=\phi'-x_1$, and an electric potential due to the

charge of the EDL, ψ (Patankar and Hu, 1998). All the variables in Eqs. (1)~(8) are nondimensionalized as follows: u_i's are normalized by the electroosmotic velocity, $U_{eo} \equiv (\varepsilon \zeta_0)/(\rho \nu)$ [ε is the fluid permittivity and $\zeta_0 (<0)$ the EDL zeta potential], x_i's by the channel half-width, H, t by H^2/D (D is the ionic diffusion coefficient), and Φ and ϕ by $-E_0 H$ [$E_0 (<0)$ is the mean external streamwise electric field], and ψ by RT/zF (R is the gas constant and T the absolute temperature). In addition, p is normalized by $\rho \nu U_{eo}/H$ (ρ is the fluid density and ν the fluid kinematic viscosity), C_p and C_m by C_0 (C_0 is the molar ionic concentration at an electrically neutral state), and ρ_e by zFC_0 (z is the valence of the cations or anions and F the Faraday constant). Note that the electrolyte solution has been already assumed to be symmetric, i.e. $z_p = -z_m = z$ and $D_p = D_m = D$. Equations (1)~(8) constitute a complete set of governing differential equations for predicting the electroosmotic flow and ionic distributions in channel with two symmetric periodic arrays of square-sectioned ribs without any assumption of the Boltzmann distribution.

As observed previously, nondimensionalization of the governing equations involves additional dimensionless physical parameters as follows: $\mathrm{Pe} = (U_{eo} H)/D$, $\mathrm{Sc} = \nu/D$, $\Omega = (-\zeta_0)/(-E_0 H)$, $\kappa = \lambda/H$, $\zeta_0^* = (-zF\zeta_0)/(RT)$, where λ is the EDL length defined as (Li, 2004)

$$\lambda = \left[\frac{\varepsilon RT}{2F^2 z^2 C_0} \right]^{1/2} \tag{9}$$

Here, Pe is the Peclet number, Sc the Schmidt number, Ω the ratio of the zeta potential to the external electric-potential difference, κ the ratio of the EDL length to the channel half-width, and ζ_0^* the nondimensional zeta potential.

Most dielectric materials obtain electric charges when they are brought into contact with an aqueous solution and various plausible explanations for such an phenomenon can be found in literature (Li, 2004). In the present study, we assume that a certain amount of cations are released from the surface into the fluid due to ionization of a surface group, resulting in a negatively charged surface. That is, the net amounts of electric charges on the surface and in the fluid are equal in strength but different in sign, leading to the following relation (Li, 2004; Kwak and Hasselbrink, 2005):

$$2(L_p + 2h)\, \kappa \zeta_0^* = \int_{A_p} \rho_e dA \tag{10}$$

where A_p is one computational domain to be explained later. Here, the zeta potential, ζ_0, are estimated to be related, using a simple dimensional analysis, to the surface electric-charge density, σ_0, as follows: $\zeta_0 = (\sigma_0 \lambda)/\varepsilon$. Note that the relation (10) has to be satisfied at every time step during all the numerical simulations.

To solve the governing differential equations (1)~(8), appropriate boundary conditions are necessary. For the computational convenience, numerical simulations are performed only on the section of one streamwise period ($0 \le x_1 \le L_p$) and the lower half-channel ($0 \le x_2 \le H = 1$) due to the geometric and physical periodicity and symmetry, respectively. For all the dependent variables (u_1, u_2, p, C_p, C_m, ϕ' and ψ), therefore, periodic boundary conditions are applied in the streamwise direction while no-gradient (or symmetric) conditions are applied at the centerline ($x_2 = H = 1$). On the other hand, the boundary conditions at the wall of the rib and channel are given as follows: no-slip condition ($u_i = 0$), no-flux condition of the cations and anions [$\partial C_p/\partial x_n = -(\zeta_0^*/\kappa) C_p$ and $\partial C_m/\partial x_n = (\zeta_0^*/\kappa) C_m$, where the subscript, n, denotes the wall-normal direction], no-penetration condition of the external electric field ($\partial \phi'/\partial x_n = \delta_{n1}$), and condition of a constant surface electric-charge density ($\partial \psi/\partial x_n = \zeta_0^*/\kappa$).

The governing differential equations (1)~(8) are integrated in time using a second-order semi-implicit fractional-step method: a third-order Runge-Kutta method (RK3) for the convection and electric body-force terms and a second-order Crank-Nicolson method for the diffusion terms. In space, on the other hand, the governing equations are resolved with a finite-volume approach on a staggered mesh and all the spatial derivatives are discretized with the second-order central difference scheme. For more efficient simulations, the computational domain is resolved spatially with

an adoption of the tangential-hyperbolic grid distribution such that a dense clustering of grid points is applied near the wall, especially around the rib, while away from the wall a coarser grid is used : the spatial resolutions used for $L_p=1$ and 0.4 are respectively $M\times N=193\times193$ and 113×193. Since only the steady state is concerned in the present study, all the simulations may be started with arbitrary initial conditions only if the steady flow fields and ionic distributions are to be analyzed.

To confirm the spatial and temporal convergence, parametric studies for the steady electroosmotic flow at $\kappa=0.2$, Pe=1 and $\Omega=1$ in the case of $L_p=1$ and $h=0.2$ have been performed and the typical results are presented in Table 1. Details of other flow conditions will be explained in the next chapter. Here, Δx_{rib} is the minimum grid size in the streamwise and transverse directions around the rib while Δt is the time step size. The table shows that even for the 1.5-time decrease in the grid size and 2-time decrease in the time-step size the relative errors are within 0.05%, that is enough negligible for the present computational purpose. It indicates that the results obtained with the chosen parameter values are well converged with respect to the spatial and temporal resolutions.

The present study is accomplished by presenting contours of the cation and anion concentrations and electric potentials, and streamlines in the steady state at different values of the EDL length and streamwise periodic length. Particularly, the EDL length is considered for the three cases : one is the nonoverlapped EDL case ($\kappa=\lambda/H\ll1$ or $\lambda<h$ where h is the rib size), another is the overlapped EDL case ($\kappa\sim1$ or $\lambda>h$), and the other is the case of equivalent EDL length and rib size ($\lambda\sim h$). In addition, the periodic length is considered for the two cases : one is the case of sufficiently large periodic length leading to as weak interaction between two adjacent ribs as possible, and the other is the case of smaller periodic length leading to stronger interaction.

Table 1 Validation of the numerical method : parametric studies for the steady electroosmotic flow at $\kappa=0.2$ in the case of $L_p=1$. Here, parenthesized are the relative errors (%) with respect to the result from $M\times N=193\times193$ and $\Delta t=0.001$. The subscripts, c and w, denote locations at $(x_1,x_2)=(0.1,1)$ and $(0.1,0.2)$, respectively

$M\times N$	Δx_{rib}	Δt	u_{1c}	C_{pw}	C_{mw}	$\psi_w-\psi_c$
193×193	0.00048	0.0010	0.5638	6.3319	0.2842	−1.5335
289×289	0.00032	0.0005	0.5638 (0.00)	6.3313 (0.01)	0.2841 (0.04)	−1.5336 (0.01)

3. Results

After verifying the numerical method, we have conducted numerical simulations on the steady electroosmotic flow in channel equipped with two symmetric periodic arrays of square-sectioned ribs when a constant electric field is externally applied in the streamwise direction. For the computational convenience, we set the rib size to be one-fifth of the channel half-width, that is $h=0.2$ in a nondimensional form, and consider a symmetric unary electrolyte, that is $z_p=-z_m=z=1$. In addition, the nondimensional zeta potential is set to be $\zeta_0^*=2.35$, the Schmidt number Sc=1000, the Peclet number Pe=1 and the ratio of the zeta potential to the external electric potential difference $\Omega=1$.

3.1 Ionic distributions and flow field

To scrutinize the ionic distributions and their corresponding flow field, numerical simulations are performed on the steady electroosmotic flow at $\kappa=0.2$ in the case of $L_p=1$ and their results are shown in Figs. 2-4. The periodic length, $L_p=1$, is chosen such that the electroosmotic flow can be affected only by a single rib by making the interaction between two adjacent ribs as weak as possible. On the other hand, the EDL length is comparable to the rib size because the two nondimensional parameters, κ and h, are equally set to be 0.2. In addition, the EDL length is not enough small that the Boltzmann-distribution assumption is valid (Qu and Li, 2000).

Figure 2 shows contours of the cation and anion concentrations, C_p and C_m, for the same flow conditions. Note that the cations have an excess of

$2(L_p+2h)\kappa\zeta_0^*$ [corresponding to $-(L_p+2h)\sigma_0$ in a dimensional form] over the anions on the computational domain (one periodic length and the lower half-channel), as known from Eq. (10). Results show that the ionic distributions are obviously periodic in the streamwise direction, implying the validation of the boundary-condition application. As seen in Fig. 2(a), the cations move toward the wall, particularly the rib, mainly due to the attractive force with the negatively charged wall and finally they are clustered around the rib with the highest concentrations on the two bottom corners. Looking more closely around the rib, the concentration of the cations is nearly constant on the top wall, and it drastically increases with going downward along the two lateral walls. On the other hand, the anions have the opposite concentration distribution to the cations because of the different electric property, as seen in Fig. 2(b). That is, the anions move from the rib toward the centerline mainly due to the repulsive force from the negatively charged wall. Consequently, the anions have the lowest concentrations on the two bottom corners. As known in Fig. 2, the concentration of the cations changes more rapidly than that of the anions across the EDL around the wall of the rib and channel.

Contours of the electric potentials are shown in Fig. 3 for the same flow conditions. At first, Fig. 3(a) shows contours of the external electric potential, $\phi=\phi'-x_1$. In the bulk of the fluid away from the rib, the contour lines are fairly evenly distributed in parallel with the transverse direction and their distribution is periodic in the streamwise direction. It indicates that a constant external electric field, -1 (corresponding to E_0 in a dimensional form), is exerted on the flow along the channel. Close to the rib, on the other hand, the contour lines are perpendicular to the wall of the rib and channel and they are more densely distributed on the top wall of the rib than on the two lateral walls. Next, Fig. 3(b) shows contours of the EDL electric potential, ψ. The Poisson equation (7) implies that the electric-potential distribution is closely related to those of the cations and anions. The volumetric electric-charge density, $\rho_e=C_p-C_m$, close to the rib is higher than in the bulk of the fluid away from the rib (see Fig. 2). Therefore, the EDL electric

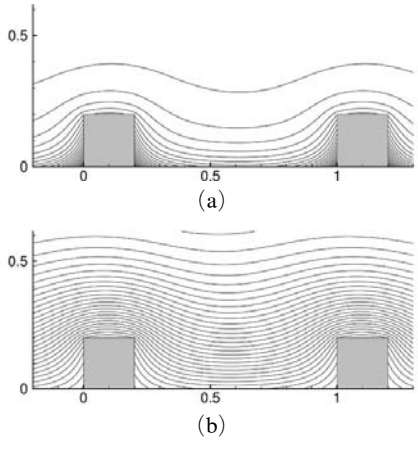

Fig. 2 Contours of the cation and anion concentrations in the steady electroosmotic flow at $\kappa=0.2$ in the case of $L_p=1$: (a) C_p ($\Delta=1$) and (b) C_m ($\Delta=0.04$). Here, Δ denotes constant contour-level increments

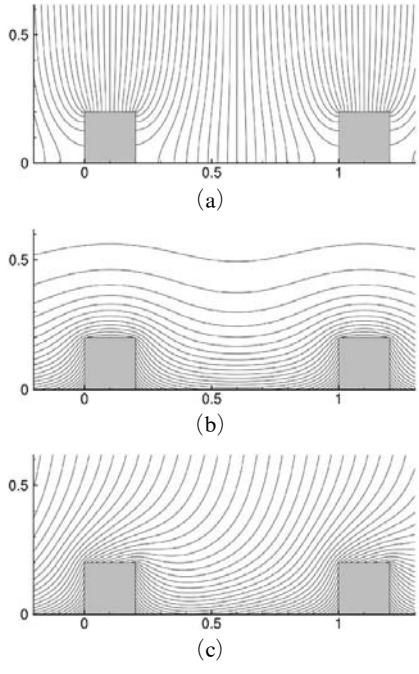

Fig. 3 Contours of the electric potentials in the steady electroosmotic flow at $\kappa=0.2$ in the case of $L_p=1$: (a) ϕ ($\Delta=0.025$), (b) ψ ($\Delta=0.05$) and (c) $\Phi=\phi+(\Omega/\zeta_0^*)\psi$ ($\Delta=0.05$). Here, Δ denotes constant contour-level increments

potential decreases with approaching the rib and attains the minimum (or maximum negative) values on the two bottom corners. Finally, Fig. 3(c) shows contours of the total electric potential obtained through Eq. (5). Close to the wall of the rib and channel, the distribution of the total electric potential resembles more that of the EDL potential, indicating the dominance of the EDL one. Far away from the wall, on the other hand, it resembles more that of the external electric potential, indicating the dominance of the external one.

As shown in Eq. (2), the electroosmotic flow can be driven through the body force term, $-\rho_e(\partial\Phi/\partial x_i)$ or $\rho_e E_i$ where $E_i=-\partial\Phi/\partial x_i$ is the total electric field, that is through the interaction between the electric-charge distribution in fluid and the total electric field. Thus, the electric body force is exerted in the direction normal to contour lines of the total electric potential. Here, it is remarkable to mention in which direction the electric body force acts. Note that the total electric field is a sum of the external electric field and the EDL one, i.e. $E_i=-\partial\phi/\partial x_i-(\Omega/\zeta_0^*)\partial\psi/\partial x_i$. Close to the rib, the electric body force is exerted toward the front bottom corner (↘) on the front side of the rib, while it is toward the back bottom corner (↙) on the back side. On the top side, the electric force is exerted downstream and downward (↘) because this region is affected comparably by the external electric field (downstream) and the EDL one (downward). Away from the rib, on the other hand, the electric force is exerted downstream and downward (↘) because of the combined effects of the external electric field and EDL one. Then, with going farther away from the wall, the downward electric-force component due to the EDL electric field diminishes and, thus, the electric force is more directed right to the downstream.

Figure 4(a) shows streamlines in the steady electroosmotic flow at $\kappa=0.2$ in the case of $L_p=1$. Here, the stream function at the wall is set to be zero. It is seen that the flow takes a spatially wavy motion because of the periodic arrays of ribs. In addition, very thin bubbles are found around the rib and their appearance is very complicated. To more closely investigate the flow pattern, enlargements of the flow field around the rib are shown in Fig. 4(b). The figures indicate that bubbles with negative values of the stream function are found on the top and front sides of the rib, whereas those with positive values are on the back side. Note that the stream function becomes negative when flow separation occurs from the wall, whereas otherwise it is positive. On the top side, flow separation occurs and a very thin recirculation bubble is formed along the wall. On the front side, a recirculation bubble of reversed-'L' shape is located along the front-side wall of the rib and the channel wall, while inside the 'L'-shape bubble a very thin and long bubble is formed along the front-side wall. On the back side, on the other hand, the flow pattern is much more complicated. The values of the stream function are all positive, indicating that flow separation does not occur on this side. The fluid that

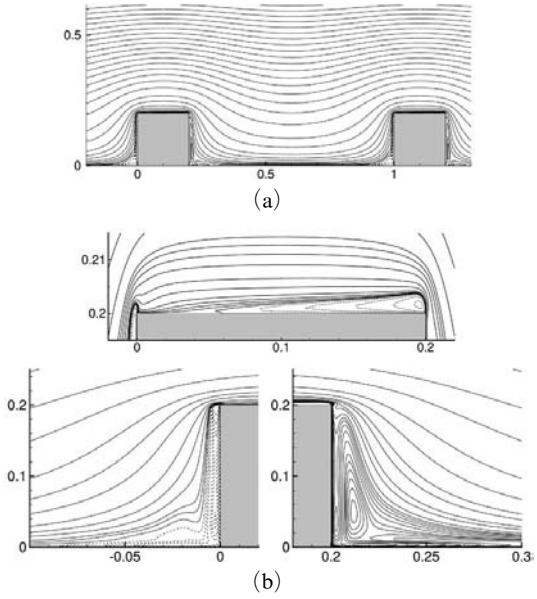

Fig. 4 Streamlines in the steady electroosmotic flow at $\kappa=0.2$ in the case of $L_p=1$: (a) over the whole domain and (b) on the top, left-hand and right-hand sides of the rib. The stream-function levels are not to scale and their negative values are dashed. Note that, in (b), the scales in the x_1 and x_2 directions are set different to comprehend the bubble structure around the rib

flows down along the back-side wall takes a big heaving and dipping motion all through the wall, leaving two slender vertical bubbles. In addition, two more slender horizontal bubbles are formed along the channel wall.

As observed in Eq. (2), the flow-driving force in the electroosmotic flow is not uniform over the flow domain because it depends strongly on the spatial distributions of the ionic species and thus electric potentials. In that sense, the electroosmotic flow should be basically different from the conventional pressure-driven flow. To confirm the difference, the same numerical simulation has been performed under an assumption that the cations and anions are uniformly distributed. For the simulation, the electric body-force term, $-(\mathrm{Sc}/2\kappa^2\zeta_0^*)\rho_e(\partial\Phi/\partial x_i)$, is replaced with the mean pressure-gradient term, $-dP/dx_i=-(\mathrm{Sc}/2\kappa^2\zeta_0^*)\langle\rho_e\rangle\langle\partial\Phi/\partial x_i\rangle$, in the momentum equation (2), where $\langle\cdot\rangle$ is the spatial averaging. Here, the average volumetric electric-charge density can be obtained from Eq. (10), that is

$$\langle\rho_e\rangle=\frac{2(L_p+2h)\,\kappa\zeta_0^*}{L_p-h^2} \tag{11}$$

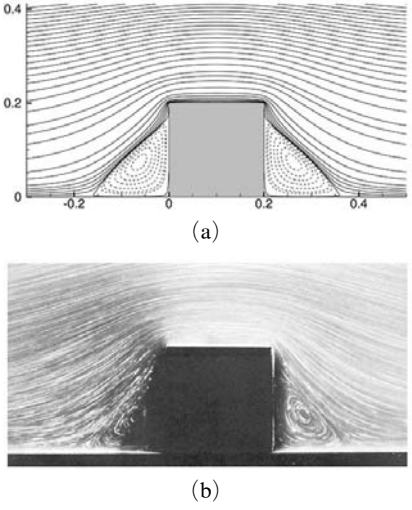

Fig. 5 Streamlines in the pressure-driven flow in the case of $L_p=1$: (a) the present numerical study for $\kappa=0.2$ and $-dP/dx_1=(\mathrm{Sc}/2\kappa^2\zeta_0^*)\langle\rho_e\rangle$ where $\langle\cdot\rangle$ is the spatial averaging, and (b) Taneda's experimental work (Van Dyke, 1982). In (a), the stream-function levels are not to scale and their negative values are dashed

while the average electric field is set to be $\langle\partial\Phi/\partial x_i\rangle=-\delta_{i1}$ [corresponding to $E_0\delta_{i1}$ in a dimensional form]. The simulation result is shown in Fig. 5(a), compared with Taneda's experimental work (Van Dyke, 1982) for the pressure-driven external flow at a very low Reynolds number, $\mathrm{Re}=0.02$ (defined by the free-stream velocity and the rib size). It is found that, despite of the difference in the flow conditions, both the flow fields are very similar in their appearance. That is, they involve two big recirculation bubbles with negative values of the stream function on the front and back sides of the rib. Therefore, it can be confirmed that such complicated electroosmotic-flow pattern around the rib shown in Fig. 4 comes from the spatially-varying ionic concentrations and thus electric potentials.

3.2 Effect of the EDL length

In this section, we discuss how the electroosmotic flow varies with changing nondimensional EDL length, κ, in channel equipped with two symmetric periodic arrays of square-sectioned ribs. For the study, numerical simulations are performed for two more EDL lengths, $\kappa=0.05$ and 1, in the case of $L_p=1$ and their results are shown in Figs. 6 and 7, respectively (see also Figs. 2-4 for comparison with the case of $\kappa=0.2$). Figures 6(a)-(c) show contours of the cation and anion concentrations and total electric potential in the steady electroosmotic flow at $\kappa=0.05$. With the choice of $\kappa=0.05$, the EDL is four times as thin as the rib, i.e. $\kappa/h=0.25$, and it is enough thin compared with the channel half-width ($\kappa=\lambda/H=0.05\ll1$) that the Boltzmann-distribution assumption is valid. As expected, the cations are clustered in a very thin EDL layer around the wall of the rib and channel mainly due to the attractive force with the negatively charged wall, and their concentration variation across the EDL is very steep compared with the case of $\kappa=0.2$. Despite the change of the EDL length, the cations still have the highest concentrations on the two bottom corners. On the other hand, the anions are repelled away from the wall mainly due to the repulsive force with the negatively charged wall. Such ionic distributions directly affect that of the

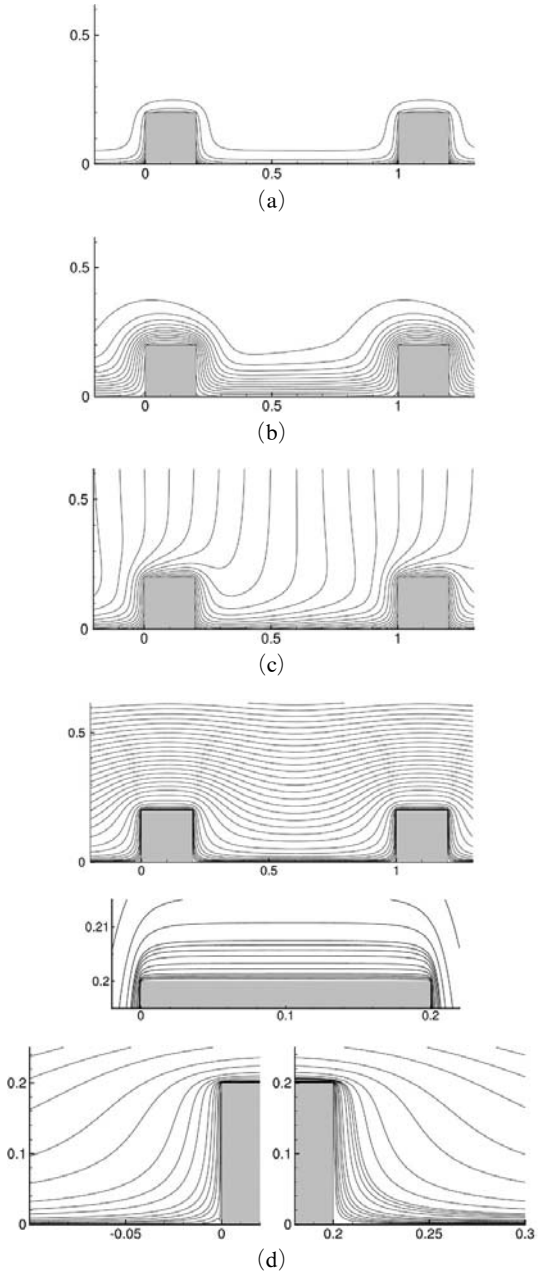

Fig. 6 (a)-(c) Contours of the cation and anion concentrations and total electric potentials and (d) streamlines in the steady electroosmotic flow at $\kappa=0.05$ in the case of $L_p=1$: (a) C_p ($\Delta=2$), (b) C_m ($\Delta=0.08$) and (c) Φ ($\Delta=0.1$). In the streamlines, the stream-function levels are not to scale and their negative values are dashed. In the contours, on the other hand, Δ denotes constant contour-level increments

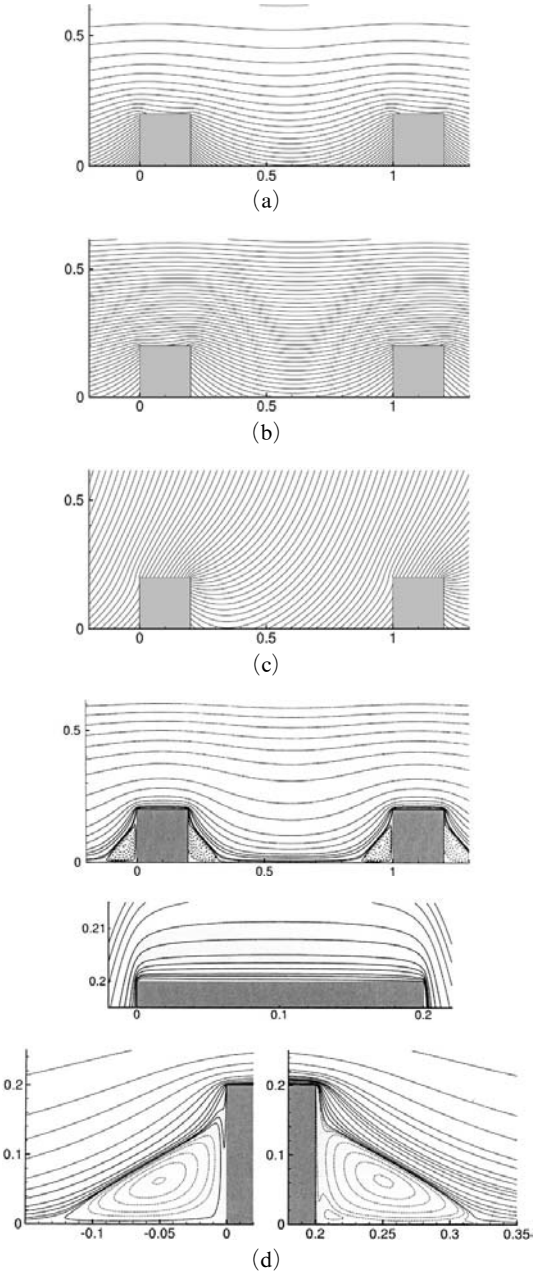

Fig. 7 (a)-(c) Contours of the cation and anion concentrations and total electric potentials and (d) streamlines in the steady electroosmotic flow at $\kappa=1$ in the case of $L_p=1$: (a) C_p ($\Delta=0.5$), (b) C_m ($\Delta=0.02$) and (c) Φ ($\Delta=0.025$). In the streamlines, the stream-function levels are not to scale and their negative values are dashed. In the contours, on the other hand, Δ denotes constant contour-level increments

electric potential [see Fig. 6(c)]. Very close to the wall, the contour lines are nearly parallel to the wall because the EDL is very thin and its effect is very strong. In the bulk of the fluid, to the contrary, the contour lines are distributed such that the total electric field is directed right to the downstream. Figure 6(d) shows streamlines in the steady electroosmotic flow at $\kappa=0.05$. It is seen that neither flow separation occurs nor any bubble structure is formed, which is totally different from the case of $\kappa=0.2$. That is, close to the wall, the fluid flows along the wall as in the inviscid flow.

Figures 7(a)-(c) show contours of the cation and anion concentrations and total electric potential in the steady electroosmotic flow at $\kappa=1$. With the choice of $\kappa=1$, the EDL is five times as thick as the rib, i.e. $\kappa/h=5$. As well, the EDL length is equal to the channel half-width, that is the whole channel is fully EDL-overlapped and thus the Boltzmann-distribution assumption cannot be applicable at all. Results show that the distributions of the ionic concentrations and electric potential are similar to the cases of thinner EDL lengths, i.e. $\kappa=0.2$ and 0.05, but their variations are much milder over the whole channel. It means that the EDL effect from the wall extends far away from the wall, that is to the whole channel. The corresponding streamlines are shown in Fig. 7(d). Two big recirculation bubbles with negative values of the stream function are formed on the front and back sides of the rib, which is similar to the case of the conventional pressure-driven flow (see Fig. 5). Since the flow belongs to the fully overlapped EDL case, the EDL effect extends to the whole channel and thus the EDL electric potential is relatively uniform. Therefore, the flow resembles more the pressure-driven flow with increasing EDL length.

3.3 Effect of the periodic length

In this section, we discuss effect of the periodic length on the steady electroosmotic flow in channel equipped with two symmetric periodic arrays of square-sectioned ribs. For the discussion, numerical simulations are performed by shortening the periodic length to $L_p=0.4$ for the three EDL lengths, $\kappa=0.05$, 0.2 and 1. With the choice of $L_p=0.4$, the interaction between two adjacent ribs becomes very strong compared with the case of $L_p=1$.

Figure 8 shows streamlines in the steady electroosmotic flow at $\kappa=0.05$ for $L_p=0.4$ (see also Fig. 6 for comparison with the case of $L_p=1$). It is seen that, at a very small EDL length, the basic characteristic in the flow pattern for $L_p=0.4$ is similar to that for $L_p=1$, that is the fluid flows along the wall as in the inviscid flow. Nevertheless, extremely thin bubbles are formed around the rib due to the stronger interaction between two adjacent ribs. In addition, in the bulk of the fluid, the fluid flows downstream less distorted by the array of ribs because of its more compact arrangement.

Apparent variation of the flow pattern with the periodic length can be observed at $\kappa=0.2$ and 1. Figures 9 and 10 show streamlines in the steady electroosmotic flow, respectively, at $\kappa=0.2$ and 1 for $L_p=0.4$. The figures show that one big recirculation bubble with negative values of the stream function is generated between two adjacent ribs and attached to the front-side wall of the rib. It is implied that, with decreasing periodic length,

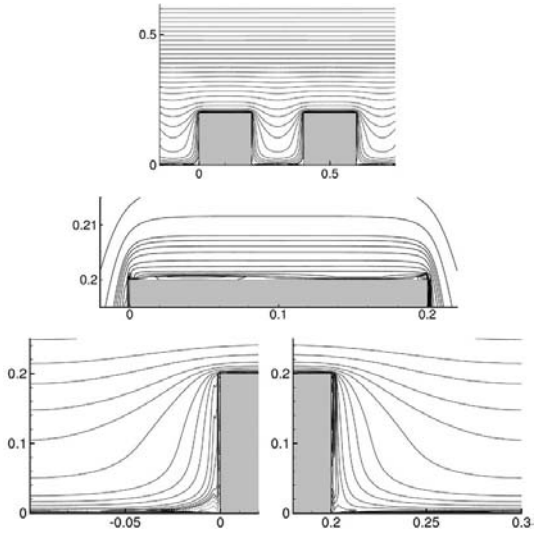

Fig. 8 Streamlines in the steady electroosmotic flow at $\kappa=0.05$ in the case of $L_p=0.4$. The stream-function levels are not to scale and their negative values are dashed

the critical EDL length above which such a bubble structure exists also decreases.

Despite such one-big-bubble structure between two adjacent ribs, the flow pattern changes more or less according to the EDL length. In the case of $\kappa=0.2$, on the back side of the rib, the fluid flows downward and then upward, leading to 'L'-shape flow pattern with positive values of the stream function. On the front side, to the contrary, a very complicated flow pattern with negative values of the stream function, composed of small bubbles and reversed-'L' shape streamlines, is formed. In the case of $\kappa=1$, however, such flow patterns become appreciably weak. In other words, with increasing EDL length, the flow pattern resembles more that of the conventional pressure-driven flow and the big bubble expands its size.

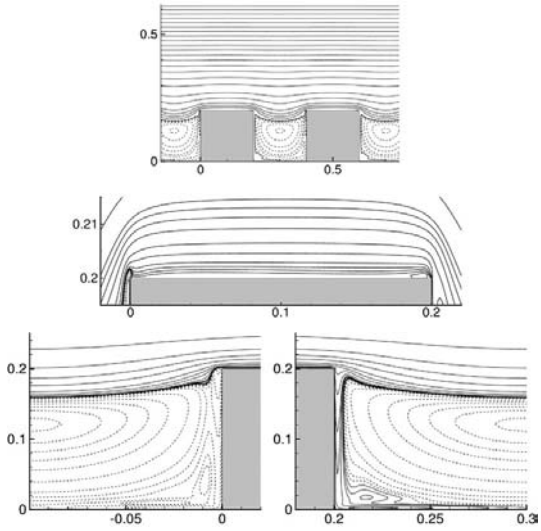

Fig. 9 Streamlines in the steady electroosmotic flow at $\kappa=0.2$ in the case of $L_p=0.4$. The stream-function levels are not to scale and their negative values are dashed

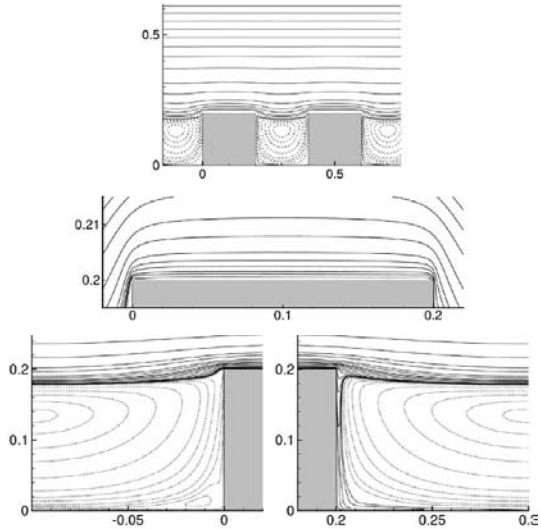

Fig. 10 Streamlines in the steady electroosmotic flow at $\kappa=1$ in the case of $L_p=0.4$. The stream-function levels are not to scale and their negative values are dashed

4. Summary

In this study, we have numerically investigated two-dimensional electroosmotic flows in channel equipped with two symmetric periodic arrays of square-sectioned ribs under the external application of a constant electric field. Here, the rib size was set to be one-fifth of the channel half-width ($h=0.2$). Such a flow geometry was chosen because transverse flows could be generated due to the interaction between the electroosmotic flow and square-sectioned ribs, probably enhancing the mixing efficiency. For the numerical study, the ionic-species and electric-potential equations as well as the continuity and momentum ones were solved using the finite volume method. Instead of assuming the Boltzmann distribution, the Nernst-Plank equation was introduced for the ionic species.

Results showed that the steady electroosmotic flow and ionic distributions depended strongly on the EDL length and streamwise periodic length. The cations moved toward the wall, particularly the rib, mainly due to the attractive force with the negatively charged wall and finally they were clustered around the rib with the highest concentrations on the two bottom corners. On the other hand, the anions moved from the rib toward the centerline mainly due to the repulsive force from the negatively charged wall. Close to the rib, the electric body force was exerted toward the front bottom corner (↘) on the front side of the rib, while it was toward the back bottom corner (↙) on the back side. With going farther away from

the rib, to the contrary, the effect of the EDL electric field became weaker and thus the electric force was more directed right to the downstream.

For a sufficiently large periodic length (L_P= 1), at the EDL length equal to the rib size (κ= h), very thin bubbles were found around the rib and their appearance was very complicated. On the front side of the rib, a recirculation bubble of reversed-'L' shape with negative values of the stream function was located along the front-side wall of the rib and the channel wall. On the back side, to the contrary, the fluid that flowed down along the back-side wall took a big heaving and dipping motion all through the wall, leaving two slender vertical bubbles. In addition, two more slender horizontal bubbles were formed along the channel wall. At a small EDL length (κ=0.05< h), neither flow separation occurred nor any bubble structure was formed. That is, close to the wall, the fluid flowed along the wall as in the inviscid flow. At a large EDL length (κ=1>h), on the other hand, two big recirculation bubbles were formed on the front and back sides of the rib as in the conventional pressure-driven flow.

As the periodic length decreased (L_P=1 to 0.4), the flow pattern changed greatly at a relatively large EDL length (κ=0.2 or 1): one big recirculation bubble was generated between two adjacent ribs and attached to the front-side wall of the rib. However, at a small EDL length (κ= 0.05), the variation was not so much. In other words, with decreasing periodic length, the critical EDL length above which such a bubble structure existed decreased. This study would contribute to further understanding electroosmotic flows and developing more feasible passive mixers in micro- and nanofluidic devices.

Acknowledgments

This work was supported by the NRL (National Research Laboratory) Program of the Ministry of Science and Technology, Korea.

References

Hu, L., Harrison, J. D. and Masliyah, J. H., 1999, "Numerical Model of Electrokinetic Flow for Capillary Electrophoresis," *Journal of Colloid and Interface Science*, Vol. 215, pp. 300~312.

Kwak, H. S. and Hasselbrink Jr., E. F., 2005, "Timescales for Relaxation to Boltzmann Equilibrium in Nanopores," *Journal of Colloid and Interface Science*, Vol. 284, pp. 753~758.

Li, D., 2004, *Electrokinetics in Microfluidics*, Elsevier, London.

Lin, H., Storey, B. D., Oddy, M. H., Chen, C.-H. and Santiago, J. G., 2004, "Instability of Electrokinetic Microchannel Flows with Conductivity Gradients," *Physics of Fluids*, Vol. 16, pp. 1922~1935.

Lin, J. Y., Fu, L. M. and Yang, R. J., 2002, "Numerical Simulation of Electrokinetic Focusing in Microfluidic Chips," *Journal of Micromechanics and Microengineering*, Vol. 12, pp. 955~961.

Liu, R. H., Stremler, M. A., Sharp, K. V., Olsen, M. G., Santiago, J. G., Adrian, R. J., Aref, H. and Beebe, D. J., 2000, "Passive Mixing in a Three-Dimensional Serpentine Microchannel," *Journal of Microelectromechanical Systems*, Vol. 9, pp. 190~197.

Patankar, N. A. and Hu, H. H., 1998, "Numerical Simulation of Electroosmotic Flow," *Analytical Chemistry*, Vol. 70, pp. 1870~1881.

Qian, S. and Bau, H. H., 2005, "Theoretical Investigation of Electro-osmotic Flows and Chaotic Stirring in Rectangular Cavities," *Applied Mathematical Modelling*, Vol. 29, pp. 726~753.

Qu, W. and Li, D., 2000, "A Model for Overlapped EDL Fields," *Journal of Colloid and Interface Science*, Vol. 224, pp. 397~407.

Stone, H. A., Stroock, A. D., and Ajdari, A., 2004, "Engineering Flows in Small Devices: Microfluidics toward a Lab-on-a-Chip," *Annual Review of Fluid Mechanics*, Vol. 36, pp. 381~411.

Stroock, A. D., Dertinger, S. K. W., Ajdari, A., Mezić, I., Stone, H. A. and Whitesides, G. M., 2002, "Chaotic Mixer for Microchannels," *Science*, Vol. 295, pp. 647~651.

Van Dyke, M., 1982, *An Album of Fluid Motion*, Parabolic Press, California.